GW190521 as a Merger of Proca Stars: A Potential New Vector Boson of 8.7×10^{-13} eV

Juan Calderón Bustillo [1,2,3,4,*] Nicolas Sanchis-Gual [5,6,†] Alejandro Torres-Forné, [7,8,9] José A. Font [8,9] Avi Vajpeyi, [3,4]
Rory Smith [3,4] Carlos Herdeiro [6] Eugen Radu, [6] and Samson H. W. Leong [2]

[1]*Instituto Galego de Física de Altas Enerxías, Universidade de Santiago de Compostela, 15782 Santiago de Compostela, Galicia, Spain*
[2]*Department of Physics, The Chinese University of Hong Kong, Shatin, N.T., Hong Kong*
[3]*Monash Centre for Astrophysics, School of Physics and Astronomy, Monash University, Victoria 3800, Australia*
[4]*OzGrav: The ARC Centre of Excellence for Gravitational-Wave Discovery, Clayton, Victoria 3800, Australia*
[5]*Centro de Astrofísica e Gravitação—CENTRA, Departamento de Física, Instituto Superior Técnico—IST,*
Universidade de Lisboa—UL, Avenida Rovisco Pais 1, 1049-001, Portugal
[6]*Departamento de Matemática da Universidade de Aveiro and Centre for Research and*
Development in Mathematics and Applications (CIDMA), Campus de Santiago, 3810-183 Aveiro, Portugal
[7]*Max Planck Institute for Gravitational Physics (Albert Einstein Institute), Am Mühlenberg 1, Potsdam 14476, Germany*
[8]*Departamento de Astronomía y Astrofísica, Universitat de València, Dr. Moliner 50, 46100, Burjassot (València), Spain*
[9]*Observatori Astronòmic, Universitat de València, C/ Catedrático José Beltrán 2, 46980, Paterna (València), Spain*

Advanced LIGO-Virgo have reported a short gravitational-wave signal (GW190521) interpreted as a quasicircular merger of black holes, one at least populating the pair-instability supernova gap, that formed a remnant black hole of $M_f \sim 142\ M_\odot$ at a luminosity distance of $d_L \sim 5.3$ Gpc. With barely visible premerger emission, however, GW190521 merits further investigation of the pre-merger dynamics and even of the very nature of the colliding objects. We show that GW190521 is consistent with numerically simulated signals from head-on collisions of two (equal mass and spin) horizonless vector boson stars (aka Proca stars), forming a final black hole with $M_f = 231^{+13}_{-17}\ M_\odot$, located at a distance of $d_L = 571^{+348}_{-181}$ Mpc. This provides the first demonstration of close degeneracy between these two theoretical models, for a real gravitational-wave event. The favored mass for the ultralight vector boson constituent of the Proca stars is $\mu_V = 8.72^{+0.73}_{-0.82} \times 10^{-13}$ eV. Confirmation of the Proca star interpretation, which we find statistically slightly preferred, would provide the first evidence for a long sought dark matter particle.

DOI: 10.1103/PhysRevLett.126.081101

Introduction.—Gravitational-wave (GW) astronomy has revealed stellar-mass black holes (BHs) more massive than those known from x-ray observations [1,2]. This population, with masses of tens of solar masses, complements the supermassive black holes (SMBHs) lurking in the center of most galaxies, with masses in the range 10^5–$10^{10}\ M_\odot$ [3]. The observation of GW190521 [4] by the Advanced LIGO [5] and Virgo [6] detectors has populated the gap between these two extremes. The LIGO-Virgo Collaboration (LVC) interprets GW190521 as a short-duration signal consistent with a quasi-circular binary black hole (BBH) merger, with mild signs of orbital precession, that left behind the first ever observed intermediate-mass black hole (IMBH), with a mass of $\sim 142\ M_\odot$ [4,7]. This interpretation is challenged by the fact that at least one of the BHs sourcing GW190521 must fall within the pair-instability supernova (PISN) gap. Alternative interpretations of GW190521 as an eccentric BBH lead to the same conclusion [8,9]. According to stellar evolution, such BHs cannot form from the collapse of a star [10], suggesting that this event is sourced by second generation BHs, born in previous mergers.

GW190521 is, however, different from previously observed signals. While consistent with a BBH merger, its premerger signal, and therefore a putative inspiral phase, is barely observable in the detectors sensitive band, motivating the exploration of alternative scenarios that do not involve an inspiral stage. One such possibility is a head-on collision (HOC), which we have recently investigated [11]. Within such geometry, however, the high spin of the GW190521 remnant, $a \sim 0.7$, is difficult to reach with mass ratios ($1 < q \equiv m_1/m_2 < 4$) due to the lack of orbital angular momentum and the Kerr limit on the BH spin ($a \le 1$), imposed by the cosmic censorship conjecture. There exist, however, exotic compact objects (ECOs) not subject to this limit that may mimic BBH signals, leading to a degeneracy in the emitted signals [12].

ECOs have been proposed, e.g., as dark-matter candidates, often invoking the existence of hypothetical ultralight (i.e., sub-eV) bosonic particles. One common candidate is the pseudoscalar QCD axion, but other ultralight bosons arise, e.g., in the string axiverse [13]. In particular, vector bosons are also motivated in extensions of the standard model of elementary particles and can clump

together forming macroscopic entities dubbed bosonic stars. These are among the simplest and dynamically more robust ECOs proposed so far and their dynamics has been extensively studied, e.g., Refs. [14–17]. Scalar boson stars and their vector analogs, Proca stars [18,19] (PSs), are self-gravitating stationary solutions of the Einstein-(complex, massive) Klein-Gordon [20] and of the Einstein-(complex) Proca [18] systems, respectively. These consist on complex bosonic fields oscillating at a well-defined frequency ω, which determines the mass and compactness of the star. Bosonic stars can dynamically form without any fine-tuned condition through the gravitational cooling mechanism [21,22]. While spinning solutions have been obtained for both scalar and vector bosons, the former are unstable against nonaxisymmetric perturbations [23]. Hence, we will focus on the vector case in this work. For non-self-interacting bosonic fields, the maximum possible mass of the corresponding stars is determined by the boson particle mass μ_V. In particular, ultralight bosons within $10^{-13} \leq \mu_V \leq 10^{-10}$ eV can form stars with maximal masses ranging between ~ 1000 and 1 solar masses, respectively.

We perform Bayesian parameter estimation and model selection on 4 sec of publicly available data [24] from the two Advanced LIGO and Virgo detectors around the time of GW190521 (for full details see the Supplemental Material [25], which includes references [26–32]). We compare GW190521 to numerical-relativity simulations of (i) HOCs, (ii) equal-mass and equal-spin head-on PS mergers (PHOCs), and (iii) to the surrogate model for generically spinning BBH mergers NRSur7dq4 [33]. Our simulations include the GW modes $(\ell, m) = (2, 0), (2, \pm 2), (3, \pm 2)$ while the BBH model contains all modes with $\ell \leq 4$. The PHOC cases we consider form a

Kerr BH with a feeble Proca remnant that does not impact on the GW emission [34]. Finally, to check the robustness of our results, we perform an exploratory study comparing GW190521 to a limited family of simulations for unequal-mass ($q \neq 1$) head-on PS mergers. For finer details on numerical simulations, we refer the reader to our Supplemental Material [25] and references [35–43] therein.

Results.—Figure 1 shows the whitened strain time series from the LIGO Livingston detector and the best fitting waveforms returned by our analyses for HOCs, PHOCs, and BBH mergers. While the latter two show a similar morphology with slight pre-peak power, the HOC signal is noticeably shorter and has a slightly larger ringdown frequency. These features are more evident in the right panel, where we show the corresponding Fourier transforms (dashed) together with the corresponding raw, non-whitened versions (solid). The HOC waveform displays a rapid power decrease at frequencies below its peak due to the absence of an inspiral. In contrast, PHOCs show a low-frequency tail due to the precollapse emission that mimics the typical inspiral signal present in the BBH case down to $f \simeq 20$ Hz. Below this limit, the putative inspiral signal from a BBH disappears behind the detector noise (dashed gray) making the signal barely distinguishable from that of a PHOC.

Figure 2 shows the two-dimensional 90% credible intervals for the redshifted final mass and the final spin obtained by the LVC using BBH models covering inspiral, merger and ringdown (IMR, in black) and solely from the ringdown emission; starting at the signal peak (gray) and 12.7 msec later (pink) [44,45]. Overlaid, we show the redshifted final mass M_f^z and spin a_f obtained by PHOC and HOC models, with the color code denoting the
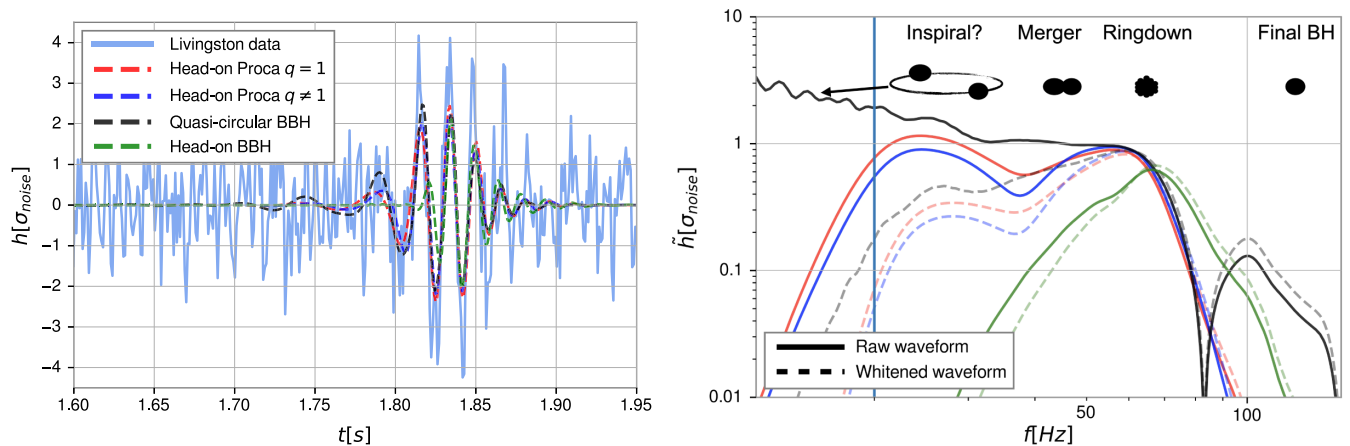

FIG. 1. Time series and spectrum of GW190521. Left: Whitened strain data of the LIGO Livingston detector at the time of GW190521, together with the best fitting waveforms for a head-on merger of two BHs (green), two equal or unequal mass PSs (red and blue) and for a quasicircular BH merger (black). The time axis is expressed so that the GPS time is equal to $t_{\mathrm{GPS}} = t + 1242442965.6069$ s. Right: corresponding waveforms shown in the Fourier domain. Solid lines denote raw waveforms (scaled by a suitable, common factor) while dashed lines show the whitened versions. The vertical line denotes the 20 Hz limit, below which the detector noise increases dramatically. Because of this, a putative inspiral signal from a quasicircular BBH merger (solid black) would be almost invisible to the detector (see dashed gray) and barely distinguishable from PHOC signals (dashed red and blue).
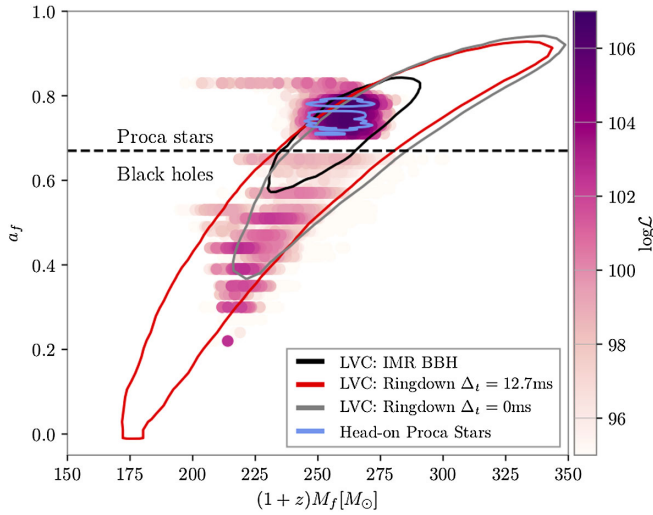
FIG. 2. Redshifted final mass and spin of GW190521 according to different waveform models, and directly inferred from a ringdown analysis. The contours delimit 90% credible intervals. For head-on PS and BH mergers (PHOCs and HOCs), we plot the samples colored according to their log likelihood. The horizontal dashed line denotes an experimental limit for the final spin of head-on BH mergers that separates them from head-on PS mergers.

log-likelihood of the corresponding samples. For these, we approximate the final mass by the total mass due to the negligible loss to GWs.

The absence of an inspiral makes HOCs and PHOCs less luminous than BBHs, therefore requiring a lower initial mass to produce the same final BH as a BBH. Accordingly, the BBH scenario yields $M_{BBH}^z = 272_{-27}^{+26} \, M_\odot$ [4,24] while the former two yield lower values of $M_{HOC}^z = 238_{-21}^{+24} \, M_\odot$ and $M_{PHOC}^z = 258_{-8}^{+6} \, M_\odot$, both consistent with those estimated by the LVC ringdown analysis, $M_{BBH,Ringdown}^z = 252_{-64}^{+63} \, M_\odot$ [4], which makes no assumption on the origin of the final BH.

There is, however, a clear separation between HOCs and BBHs/PHOCs in terms of the final spin. Cosmic censorship imposes a bound $a \leq 1$ on the BHs' dimensionless spins [46]. This, together with the negligible orbital angular momentum of HOCs, prevents the production a final BH with the large spin predicted by BBH models. By contrast, PSs are not constrained by $a \leq 1$ and can form remnant BHs with higher spins from head-on collisions. Consequently, the final spin and redshifted mass predicted by PHOCs coincide with those predicted by BBH models. In addition, the discussed lack of pre-peak power in HOCs leads to a poor signal fit that penalizes the model. In Table I we report the Bayesian evidence for our source models. We obtain a relative natural log Bayes factor $\log \mathcal{B}_{BBH}^{HOC} \sim -4.2$ that allows us to confidently discard the HOC scenario.

Unlike BHs, neutron star and PS mergers do not directly form a ringing BH. Instead, a remnant transient object produces GWs before collapsing to a BH, leaving an

TABLE I. Bayesian evidence for our GW190521 source models. We report the natural log Bayes factor obtained for our different waveform models and corresponding maximum values of the log likelihood. We note that parameter estimation codes *are not* designed to find the true maximum of the likelihood, so that the values we report should be considered as approximate.

Waveform model	$\log \mathcal{B}$	$\log \mathcal{L}_{max}$
Quasicircular binary black hole	80.1	105.2
Head-on equal-mass Proca stars	80.9	106.7
Head-on unequal-mass Proca stars	82.0	106.5
Head-on binary black Hole	75.9	103.2

imprint in the GWs that is not present for HOCs, before emitting the characteristic ringdown signal. For this reason, PHOCs do not only lead to a final mass and spin fully consistent with the LVC BBH analysis but also provide a better fit to the data than HOCs, reflected by a larger maximum likelihood in Table I.

While BBHs lose around 7% of their mass to GWs, head-on mergers radiate only $\sim 0.1\%$ of it, leading to much lower distance estimates, and consequently, to much larger source-frame masses. Whereas the LVC reports a luminosity distance of $d_L \sim 5.3_{-2.6}^{+2.4}$ Gpc [4], our PHOC scenario yields $d_L = 571_{-181}^{+348}$ Mpc, similar to GW150914 [1]. Consequently, we estimate a source-frame final mass of $\sim 231_{-17}^{+13} \, M_\odot$, 62% larger than the $142_{-16}^{+28} \, M_\odot$ reported by the LVC. The lower distance estimate handicaps the PHOC model with respect to the BBH one if a uniform distribution of sources in the Universe is assumed. Nonetheless, Table I reports a $\log \mathcal{B}_{BBH}^{PHOC} \sim 0.8$, slightly favoring the PHOC model. Relaxing this assumption leads to an increased $\log \mathcal{B}_{BBH}^{PHOC} \sim 3.4$ (see Supplemental Material [25] Table I for further details when using this alternative prior). The evidence for the PHOC model is accompanied by a better fit to the data. In addition, BBHs span a significantly larger parameter space that may penalize this model. While we explored several simplifications of the BBH model (see Supplemental Material [25]), no statistical preference for the BBH scenario was obtained. We therefore conclude that, however exotic, the PHOC scenario is slightly preferred despite being intrinsically disfavoured by our standard source-distribution prior.

Unlike BBH signals [47], head-on ones are not dominated by the quadrupole $(\ell, m) = (2, \pm 2)$ modes but have a co-dominant (2,0) mode [48,49]. By repeating our analysis removing the (2,0) from our waveforms, we obtain $\log \mathcal{B}_{No(2,0)}^{(2,0)} = 0.6$ in favor of its presence in the signal. The asymmetries introduced by this mode also allow us to constrain the azimuthal angle φ describing the projection of the line-of-sight onto the collision plane, normal to the final spin. We estimate $\varphi = 0.65_{-0.54}^{+0.86}$ rad measured from the collision axis, in the direction of any of the two spins
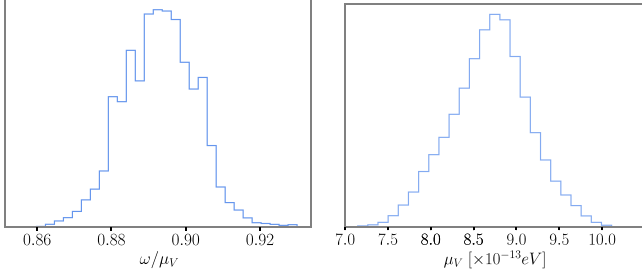
FIG. 3. Posterior distribution for the values of the bosonic field associated with GW190521. The left panel shows the oscillation frequency of the bosonic field ω/μ_V. The right panel shows the mass of the ultralight boson μ_V. We assume a merger of two equal-mass and equal-spin Proca stars.

(see Supplemental Material [25], which includes references [50–54]). This is, we restrict φ to the first and third quadrant of the collision plane, towards where the trajectories of both stars are curved due to frame dragging. To the best of our knowledge, this is the first time such measurement is performed.

We investigate the physical properties of the hypothetical bosonic field encoded in GW190521. Figure 3 shows our posterior distributions for the oscillation frequency (normalized to the boson mass) and for the boson mass μ_V itself. We constrain the former to be $\omega/\mu_V = 0.893^{+0.015}_{-0.015}$.

To obtain the boson mass μ_V one must recall that each PS model is characterized by a dimensionless mass $\mathcal{M}_{PS} = M_{PS}\mu_V/M_{Pl}^2$, with M_{Pl} the Planck mass. Identifying M_{PS} with half the mass of the final BH in GW190521 we obtain

$$\mu_V = 1.34 \times 10^{-10} \left(\frac{\mathcal{M}_{PS}}{M_{BH}^{final}/2}\right) \text{ eV}, \qquad (1)$$

where M_{BH}^{final} should be expressed in solar masses. This yields $\mu_V = 8.72^{+0.73}_{-0.82} \times 10^{-13}$ eV.

Finally, we estimate the maximum possible mass for a PS described by such ultralight boson using

$$\left(\frac{M_{max}}{M_\odot}\right) = 1.125 \left(\frac{1.34 \times 10^{-10} \text{ eV}}{\mu_V}\right). \qquad (2)$$

This yields $M_{max} = 173^{+19}_{-14} M_\odot$. Binaries with lower total masses than this M_{max} would produce a remnant that would not collapse to a BH; therefore, they would not emit a ringdown signal mimicking that of a BBH. We therefore discard PSs characterized by the above μ_V as sources of any of the previous Advanced LIGO-Virgo BBH observations, as the largest (redshifted) total mass among these, corresponding to GW170729, is only around 120 $M_\odot$ [2,53].

While our PHOC analysis is limited to equal-masses and spins, we performed a preliminary exploration of unequal-mass cases. To do this, we fix the primary oscillation frequency to $\omega_1/\mu_V = 0.895$, varying ω_2/μ_V along an

TABLE II. Parameters of GW190521 assuming a head-on merger of Proca stars. In the first column we assume equal masses and spins while the second corresponds to our exploratory model for unequal masses. There, the asterisk ($*$) denotes that we estimate the oscillation frequency of the secondary bosonic field ω_2/μ_V, while that for the primary star is fixed to $\omega_1/\mu_V = 0.895$. We report median values and symmetric 90% credible intervals.

Parameter	$q = 1$ model	$q \neq 1$ model
Primary mass	$115^{+7}_{-8} M_\odot$	$115^{+7}_{-8} M_\odot$
Secondary mass	$115^{+7}_{-8} M_\odot$	$111^{+7}_{-15} M_\odot$
Total or final mass	$231^{+13}_{-17} M_\odot$	$228^{+17}_{-15} M_\odot$
Final spin	$0.75^{+0.08}_{-0.04}$	$0.75^{+0.08}_{-0.04}$
Inclination $\pi/2 - |\iota - \pi/2|$	$0.83^{+0.23}_{-0.47}$ rad	$0.58^{+0.40}_{-0.39}$ rad
Azimuth	$0.65^{+0.86}_{-0.54}$ rad	$0.78^{+1.23}_{-1.20}$ rad
Luminosity distance	571^{+348}_{-181} Mpc	700^{+292}_{-279} Mpc
Redshift	$0.12^{+0.05}_{-0.04}$	$0.14^{+0.06}_{-0.05}$
Total or final redshifted mass	$258^{+9}_{-9} M_\odot$	$261^{+10}_{-11} M_\odot$
Bosonic field frequency ω/μ_V	$0.893^{+0.015}_{-0.015}$	$(*)0.905^{+0.012}_{-0.042}$
Boson mass μ_V [$\times 10^{-13}$]	$8.72^{+0.73}_{-0.82}$ eV	$8.59^{+0.58}_{-0.57}$ eV
Maximal boson star mass	$173^{+19}_{-14} M_\odot$	$175^{+13}_{-11} M_\odot$

uniform grid. Table II reports our parameter estimates, fully consistent with those for the equal-mass case. We obtain, however, a slightly larger evidence of $\log \mathcal{B}_{BBH}^{PHOC} = 1.9$ that we attribute to the larger distance estimate $d_L = 700^{+292}_{-279}$ Mpc. This indicates that a more in-depth exploration of the full parameter space may be of interest, albeit not impacting significantly on our main findings.

Discussion.—We have compared GW190521 to numerical simulations of BH head-on mergers and horizonless bosonic stars known as PSs. While we discard the first scenario, we have shown that GW190521 is consistent with an equal-mass head-on merger of PSs, inferring an ultralight boson mass $\mu_V \simeq 8.72 \times 10^{-13}$ eV.

Current constraints on the boson mass are obtained from the lack of GW emission associated with the superradiance instability and from observations of the spin of astrophysical BHs [55–57]. These, however, apply to *real* bosonic fields. For complex bosonic fields, the corresponding cloud around the BH does not decay by GW emission, but a stationary and axisymmetric Kerr BH with bosonic hair forms [58–60]. These configurations are, themselves, unstable against superradiance [61], but the nonlinear development of the instability is too poorly known to establish meaningful constraints on the complex bosons: see, however Ref. [62].

Our study is limited to head-on mergers of bosonic stars due to the current lack of methods to simulate less eccentric configurations. Remarkably, however, these suffice to fit

GW190521 as closely as state-of-the art BBH models, being slightly favoured from a Bayesian point of view. While this restriction leads to narrow parameter distributions, the future development of more complex configurations like quasicircular mergers shall reveal, for instance, a larger range of boson masses consistent with GW190521. This could potentially reduce the corresponding bound on the maximum mass of a stable boson star, M_{max}, and make some of the previous LIGO-Virgo events candidates for mergers of Proca stars with a compatible boson-mass μ_V. To numerically simulate such configurations, however, constraint-satisfying initial data are needed to obtain accurate waveforms, which are currently unavailable. We believe that our results will strongly motivate efforts to build such initial data.

The existence of an ultralight bosonic field would have profound implications. It could account for, at least, part of dark matter, as it would give rise to a remarkable energy extraction mechanism from astrophysical spinning BHs, eventually forming new sorts of "hairy" BHs. In addition, such field could serve as a guide towards beyond-the-standard-model physics, possibly pointing to the stringy axiverse.

While GW190521 does not allow to clearly distinguish between the BBH and PS scenarios, future GW observations in the IMBH range shall allow to better resolve the nature of the source, helping confirm or reject the existence of the ultralight vector boson discussed here.

---

*juan.calderon.bustillo@gmail.com
†nicolas.sanchis@tecnico.ulisboa.pt

[1] B. P. Abbott *et al.* (Virgo and LIGO Scientific Collaborations), Phys. Rev. Lett. **116**, 061102 (2016).
[2] B. P. Abbott *et al.* (LIGO Scientific and Virgo Collaborations), Phys. Rev. X **9**, 031040 (2019).
[3] M. Volonteri, Astron. Astrophys. Rev. **18**, 279 (2010).
[4] Abbott *et al.* (LIGO Scientific and Virgo Collaborations), Phys. Rev. Lett. **125**, 101102 (2020).
[5] J. Aasi *et al.*, Classical Quantum Gravity **32**, 115012 (2015).
[6] F. Acernese *et al.* (Virgo Collaboration), Classical Quantum Gravity **32**, 024001 (2015).
[7] B. Abbott *et al.* (LIGO Scientific and Virgo Collaborations), Astrophys. J. Lett. **900**, L13 (2020).
[8] I. M. Romero-Shaw, P. D. Lasky, E. Thrane, and J. Calderon Bustillo, Astrophys. J. Lett. **903**, L5 (2020).
[9] V. Gayathri *et al.*, arXiv:2009.05461.
[10] A. Heger, C. L. Fryer, S. E. Woosley, N. Langer, and D. H. Hartmann, Astrophys. J. **591**, 288 (2003).
[11] J. Calderon Bustillo, N. Sanchis-Gual, A. Torres-Forné, and J. A. Font, arXiv:2009.01066.
[12] V. Cardoso and P. Pani, Living Rev. Relativity **22**, 4 (2019).
[13] A. Arvanitaki, S. Dimopoulos, S. Dubovsky, N. Kaloper, and J. March-Russell, Phys. Rev. D **81**, 123530 (2010).
[14] S. L. Liebling and C. Palenzuela, Living Rev. Relativity **20**, 5 (2017).
[15] M. Bezares, C. Palenzuela, and C. Bona, Phys. Rev. D **95**, 124005 (2017).
[16] C. Palenzuela, P. Pani, M. Bezares, V. Cardoso, L. Lehner, and S. Liebling, Phys. Rev. D **96**, 104058 (2017).
[17] N. Sanchis-Gual, C. Herdeiro, J. A. Font, E. Radu, and F. Di Giovanni, Phys. Rev. D **99**, 024017 (2019).
[18] R. Brito, V. Cardoso, C. A. Herdeiro, and E. Radu, Phys. Lett. B **752**, 291 (2016).
[19] N. Sanchis-Gual, C. Herdeiro, E. Radu, J. C. Degollado, and J. A. Font, Phys. Rev. D **95**, 104028 (2017).
[20] F. E. Schunck and E. W. Mielke, Classical Quantum Gravity **20**, R301 (2003).

[21] E. Seidel and W.-M. Suen, Phys. Rev. Lett. **72,** 2516 (1994).

[22] F. Di Giovanni, N. Sanchis-Gual, C. A. R. Herdeiro, and J. A. Font, Phys. Rev. D **98,** 064044 (2018).

[23] N. Sanchis-Gual, F. Di Giovanni, M. Zilhão, C. Herdeiro, P. Cerdá-Durán, J. A. Font, and E. Radu, Phys. Rev. Lett. **123,** 221101 (2019).

[24] Abbott *et al.*, Gravitational wave open science center strain data release for gw190521, LIGO open science center (2020).

[25] See Supplemental Material at http://link.aps.org/supplemental/10.1103/PhysRevLett.126.081101 for details on the impact of prior choices in our analysis.

[26] G. Ashton *et al.*, Astrophys. J. Suppl. **241,** 27 (2019).

[27] J. Veitch, W. Del Pozzo, and M. Pitkin; https://doi.org/10.5281/zenodo.592884.

[28] N. J. Cornish and T. B. Littenberg, Classical Quantum Gravity **32,** 135012 (2015).

[29] N. J. Cornish and T. B. Littenberg, Classical Quantum Gravity **32,** 135012 (2015).

[30] L. S. Finn, Phys. Rev. D **46,** 5236 (1992).

[31] J. D. Romano and N. J. Cornish, Living Rev. Relativity **20** (2017), https://doi.org/10.1007/s41114-017-0004-1.

[32] C. Cutler and É. E. Flanagan, Phys. Rev. D **49,** 2658 (1994).

[33] V. Varma, S. E. Field, M. A. Scheel, J. Blackman, D. Gerosa, L. C. Stein, L. E. Kidder, and H. P. Pfeiffer, Phys. Rev. Research **1,** 033015 (2019).

[34] N. Sanchis-Gual, M. Zilhão, C. Herdeiro, F. Di Giovanni, J. A. Font, and E. Radu, Phys. Rev. D **102,** 101504 (2020).

[35] Einstein toolkit: http://www.einsteintoolkit.org.

[36] F. Loffler, J. Faber, E. Bentivegna, T. Bode, P. Diener *et al.*, Classical Quantum Gravity **29,** 115001 (2012).

[37] M. Zilhão and F. Löffler, Int. J. Mod. Phys. A **28,** 1340014 (2013).

[38] E. Schnetter, S. H. Hawley, and I. Hawke, Classical Quantum Gravity **21,** 1465 (2004).

[39] Cactus: http://www.cactuscode.org.

[40] M. Ansorg, B. Brügmann, and W. Tichy, Phys. Rev. D **70,** 064011 (2004).

[41] H. Witek, M. Zilhao, G. Ficarra, and M. Elley, Canuda: A public numerical relativity library to probe fundamental physics (2020).

[42] M. Zilhao, H. Witek, and V. Cardoso, Classical Quantum Gravity **32,** 234003 (2015).

[43] C. Reisswig and D. Pollney, Classical Quantum Gravity **28,** 195015 (2011).

[44] G. Carullo, W. Del Pozzo, and J. Veitch, Phys. Rev. D **99,** 123029 (2019).

[45] M. Isi, M. Giesler, W. M. Farr, M. A. Scheel, and S. A. Teukolsky, Phys. Rev. Lett. **123,** 111102 (2019).

[46] R. M. Wald, in Black Holes, Gravitational Radiation and the Universe: Essays in Honor of C.V. Vishveshwara (1997), pp. 69–85 [arXiv:gr-qc/9710068].

[47] M. Maggiore, *Gravitational Waves: Volume 1: Theory and Experiments* (OUP Oxford, New York, 2008).

[48] P. Anninos, D. Hobill, E. Seidel, L. Smarr, and W.-M. Suen, Phys. Rev. D **52,** 2044 (1995).

[49] C. Palenzuela, I. Olabarrieta, L. Lehner, and S. L. Liebling, Phys. Rev. D **75,** 064005 (2007).

[50] P. B. Graff, A. Buonanno, and B. S. Sathyaprakash, Phys. Rev. D **92,** 022002 (2015).

[51] J. Calderon Bustillo, J. A. Clark, P. Laguna, and D. Shoemaker, Phys. Rev. Lett. **121,** 191102 (2018).

[52] J. Calderon Bustillo, C. Evans, J. A. Clark, G. Kim, P. Laguna, and D. Shoemaker, Commun. Phys. **3,** 176 (2020).

[53] K. Chatziioannou *et al.*, Phys. Rev. D **100,** 104015 (2019).

[54] LIGO Scientific Collaboration, Phys. Rev. D **102,** 043015 (2020).

[55] M. Baryakhtar, R. Lasenby, and M. Teo, Phys. Rev. D **96,** 035019 (2017).

[56] V. Cardoso, Ó. J. Dias, G. S. Hartnett, M. Middleton, P. Pani, and J. E. Santos, J. Cosmol. Astropart. Phys. 03 (2018) 043.

[57] C. Palomba, S. D'Antonio, P. Astone, S. Frasca, G. Intini, I. La Rosa, P. Leaci, S. Mastrogiovanni, A. L. Miller, F. Muciaccia *et al.*, Phys. Rev. Lett. **123,** 171101 (2019).

[58] C. A. R. Herdeiro and E. Radu, Phys. Rev. Lett. **112,** 221101 (2014).

[59] C. Herdeiro, E. Radu, and H. Runarsson, Classical Quantum Gravity **33,** 154001 (2016).

[60] W. E. East and F. Pretorius, Phys. Rev. Lett. **119,** 041101 (2017).

[61] B. Ganchev and J. E. Santos, Phys. Rev. Lett. **120,** 171101 (2018).

[62] J. C. Degollado, C. A. Herdeiro, and E. Radu, Phys. Lett. B **781,** 651 (2018).

[63] https://dcc.ligo.org/P2000158-v4